Journal of Power Sources 185 (2008) 13–18

Contents lists available at ScienceDirect

Journal of Power Sources

journal homepage: www.elsevier.com/locate/jpowsour

Novel nano-network cathodes for solid oxide fuel cells

Fei Zhao[a,b], Zhiyong Wang[a], Mingfei Liu[a], Lei Zhang[a], Changrong Xia[a,*], Fanglin Chen[b]

[a] Laboratory for Renewable Clean Energy, Department of Materials Science and Engineering, University of Science and Technology of China, Hefei 230026, Anhui, China
[b] Department of Mechanical Engineering, University of South Carolina, Columbia, SC 29208, USA

ARTICLE INFO

Article history:
Received 10 June 2008
Received in revised form 13 July 2008
Accepted 15 July 2008
Available online 22 July 2008

Keywords:
Nano-network
$Sm_{0.5}Sr_{0.5}CoO_{3-\delta}$ cathode
Solid oxide fuel cells

ABSTRACT

A novel nano-network of $Sm_{0.5}Sr_{0.5}CoO_{3-\delta}$ (SSC) is successfully fabricated as the cathodes for intermediate-temperature solid oxide fuel cells (SOFCs) operated at 500–600 °C. The cathode is composed of SSC nanowires formed from nanobeads of less than 50 nm thus exhibiting high surface area and porosity, forming straight path for oxygen ion and electron transportation, resulting in high three-phase boundaries, and consequently showing remarkably high electrode performance. An anode-supported cell with the nano-network cathode demonstrates a peak power density of 0.44 W cm^{-2} at 500 °C and displays exceptional performance with cell operating time. The result suggests a new direction to significantly improve the SOFC performance.

1. Introduction

Solid oxide fuel cells (SOFCs) are among the most promising devices for environmentally clean electricity generation using different fuels such as hydrogen and hydrocarbons. However, SOFCs are currently not economically competitive due to the problems associated mainly with high temperature (>800 °C) operation, including degradation of cell components and high cost of the interconnecting materials [1]. Significant efforts thus have been devoted to lowering the operating temperature for the development of intermediate and low temperature SOFCs. At low temperatures, SOFC resistance increases rapidly and is often dominated by the interfacial polarization resistance between the electrolyte and the cathode. Accordingly, the SOFC resistance could be substantially reduced by developing novel cathode materials and/or unique microstructures to lower the interfacial polarization resistance [2,3]. To date, several new electrode architectures have been developed to create novel structures to achieve high SOFC performances at low temperatures. Among these, nanostructured electrodes are most attractive since the microstructures in nanometer scale will make available larger three-phase boundaries (TPBs) for the electrocatalytic processes of oxygen reduction. The nanostructured electrodes are typically formed by incorporating nanoparticles to preformed porous electrode frames with an ion-impregnation process involving adsorption and subsequent decomposition of metal salts [4–7]. This process usually generates 25–300 nm granular particulates randomly located on the inner surfaces of the frame [5]. The nanoscale granular particles are believed to be the primary reason for the high SOFC performance. For example, Yamahara et al. [8] studied the performance of SOFCs based on $La_{0.65}Sr_{0.30}MnO_{3-\delta}/Sc_{0.2}Y_{0.02}Zr_{0.89}O_2$ cathodes. When the cathode was incorporated with the nanostructured cobalt oxides, a power density of 0.27 W cm^{-2} was generated at 700 °C, much higher than 0.13 W cm^{-2}, which was obtained with a normal cathode. Jiang et al. [9] reported that the addition of coated nanoscale $Gd_{0.2}Ce_{0.8}O_{1.9}$ particles into a $La_{1-x}Sr_xMnO_{3-\delta}$ electrode reduced the electrode polarization resistance from 26 to 0.72 Ω cm^2 at 700 °C. Our previous work showed that cathodes impregnated with 50 nm $La_{0.6}Sr_{0.4}CoO_{3-\delta}$ particles had not only improved the electrochemical activity, but also demonstrated excellent durability upon thermal cycling and testing for 100 days [7]. High stability was also reported by Sholklapper et al. [10] for the nanoparticulate $La_{1-x}Sr_xMnO_{3-\delta}$ electrodes, where stable cell performance was observed for over 500 h of operation at 650 °C under a near-constant applied current density of ~150 mA cm^{-2}.

In this work, we report a nano-network of typical cathode material, $Sm_{0.5}Sr_{0.5}CoO_{3-\delta}$ (SSC), for low-temperature SOFC applications. The nano-network is consisted of well-connected SSC nanowires, forming straight conducting path for oxygen-ion and electron conduction. In addition, the nano-network has high porosity and the SSC nanowires are composed of SSC nanobeads. Such a cathode microsturcture shows extremely high cathode performance.

* Corresponding author. Tel.: +86 5513607475; fax: +86 5513606689.
E-mail address: xiacr@ustc.edu.cn (C.R. Xia).

0378-7753/$ – see front matter © 2008 Elsevier B.V. All rights reserved.
doi:10.1016/j.jpowsour.2008.07.022

2. Experimental

2.1. Powder preparation

Powders of $Sm_{0.2}Ce_{0.8}O_{1.9}$ (SDC) electrolyte were prepared using a glycine-nitrate process [11]. Stoichiometric amounts of $Ce(NO_3)_3{\cdot}6H_2O$ and $Sm(NO_3)_3{\cdot}6H_2O$ were dissolved in distilled water, to which glycine was added. The mixture was heated on a hot plate, evaporated to a brown-red gel, spontaneously ignited to flame, and finally converted to pale-yellow ashes, which were subsequently calcined at 800 °C for 2 h to form fluorite SDC powders. NiO powders were also synthesized using the glycine-nitrate process and were calcined at 600 °C for 2 h to remove possible organic residues.

2.2. Anode substrate formation

Substrates consisting of 60 wt.% NiO and 40 wt.% SDC were fabricated with die pressing. NiO, SDC, and a pore former (20 wt.% graphite) were mixed and ball-milled for 24 h. The mixed powders were pressed uniaxially into pellets with a diameter of 15 mm, followed by firing at 600 °C for 2 h to form porous substrates.

2.3. Electrolyte deposition

SDC electrolyte films were deposited with a suspension-coating method. SDC powders were ball-milled with organic dispersant and absolute ethanol for 48 h to form a stable suspension. The suspension was then drop-coated onto the substrates with an injector. The electrolyte thickness was controlled by the suspension volume. To avoid cracks formation as induced from evaporation of the organics, the film should be dried in an ethanol ambience.

2.4. Cathode frame fabrication

SDC frames were subsequently prepared on the deposited films with a screen-printing process. SDC slurry was prepared by ball-milling SDC powders, graphite, and ethyl cellulose-terpineol for 24 h. The slurry was then screen-printed onto the as-prepared SDC film, forming a green tri-layer structure, which was subsequently co-sintered at 1400 °C for 5 h to form a ceramic pellet consisting of a porous NiO–SDC anode substrate (~0.7 mm), a dense SDC electrolyte film (~10 μm), and a layer of porous SDC frame (~100 μm).

2.5. Cathode nano-network incorporation

$Sm_{0.5}Sr_{0.5}CoO_{3-\delta}$ nano-network was incorporated into the porous SDC frame by an ion-impregnation method. Nitrate solution, which was prepared by dissolving $Sm(NO_3)_3{\cdot}6H_2O$, $Sr(NO_3)_2$, and $Co(NO_3)_2{\cdot}6H_2O$ in distilled water at a molar ratio of Sm:Sr:Co = 0.5:0.5:1, was impregnated into the SDC frame and then fired at 700 °C for 10 min with a heating and cooling rate of 5, 10, and 20 °C min^{-1}. SSC loading was about 0.75 of the weight of the SDC frame after three impregnation-heating cycles. The impregnated product was finally fired at 800 °C for 2 h to form the desired perovskite phase. Single cells were therefore formed with cathodes consisted of SSC nano-networks within the SDC frames. A scanning electron microscope, JSM-6700F, was used to reveal the microstructure of the cell.

2.6. Cell characterization

The single cell was attached and sealed on an alumina tube by using a silver paste. The cell was tested with the humidified hydrogen (3% H_2O, 60 ml min^{-1}) as the fuel and the ambient air as the oxidant. The cell was heated to 600 °C and NiO was reduced to Ni in situ. The cell was stabilized at 600 °C for 2 h before the electrochemical test was performed. The power output performances and AC impedance spectra were measured, using a ZAHNER IM6e electrochemical station with a frequency range from 0.01 Hz to 1 MHz and a 10 mV AC perturbation. Cell performance durability test was conducted in the potentiostatic mode at a cell voltage of 0.5 V.

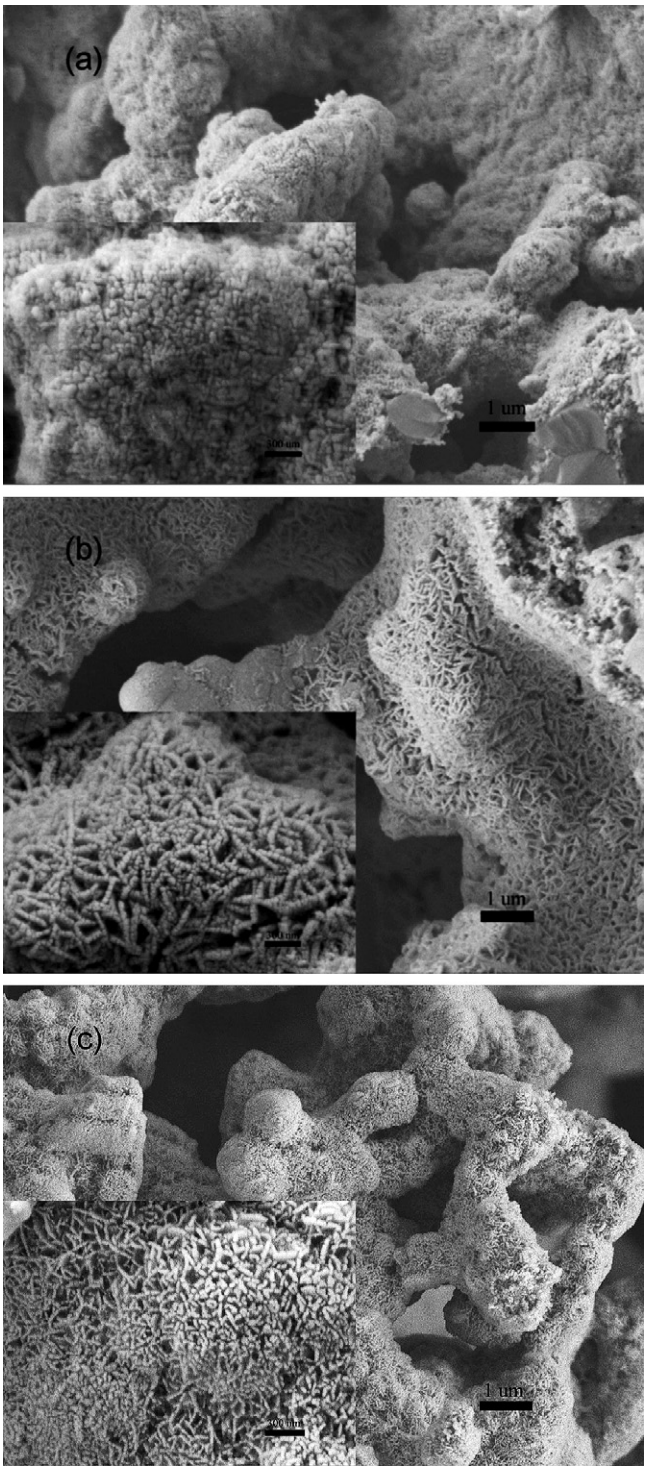

Fig. 1. Cross-sectional microstructures for cathodes with impregnated SSC fired at different heating rates: (a) 5 °C min^{-1}, (b) 10 °C min^{-1}, and (c) 20 °C min^{-1}.

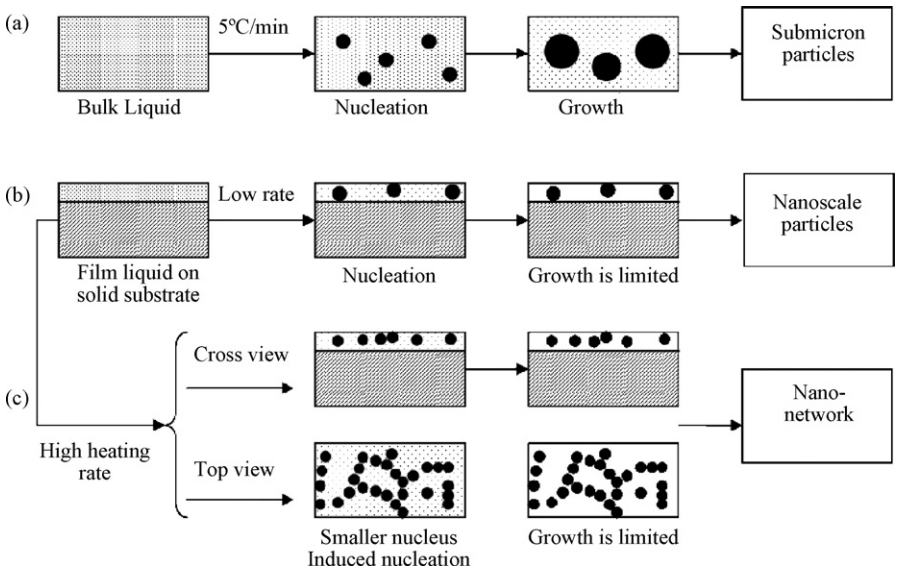

Fig. 2. Schematic diagrams for the formation of nano-networks. (a) Formation of submicron particles within bulk liquid, (b) formation of nano-particulates from a thin layer of liquid at a low heating rate, and (c) formation of nano-network from a thin layer of liquid at a high heating rate.

3. Results and discussions

3.1. Microstructure of the nano-network

Shown in Fig. 1 are the cross-section microstructures for cathodes with impregnated SSC fired at different heating rates. With a heating rate of 5 °C min^{-1}, SSC nanobeads with an average diameter of about 55 nm were randomly distributed on the inner surface of the porous SDC frame (Fig. 1a). When the heating rate was increased to 10 °C min^{-1}, the size of the SSC nanobeads decreased to about 46 nm in diameter (Fig. 1b). However, the SSC nanobeads were not randomly distributed anymore, but formed SSC nanowires composed of 5–8 SSC nanobeads. The boundary between neighboring SSC nanobeads can be easily identified. Fig. 1b also shows that the SSC nanowires are randomly oriented but interlaced, forming a porous nano-network, where the SSC nanowires construct a connected mixed ionic–electronic conducting path that is essentially important for the cathodic reaction. The unique nano-network structure was also formed when the rate was further increased to 20 °C min^{-1} (Fig. 1c). Meanwhile, the average size of the SSC nanobeads was reduced to about 38 nm. The decrease in the size of the SSC nanobeads as a result of the increased heating rate will certainly enlarge the cathode surface area, and consequently promote the rate of the electrochemical oxygen reduction in the cathode [5]. Additionally, Fig. 1b and c show that the SSC nano-network is more porous than that of the randomly distributed nanobeads structure as shown in Fig. 1a. High porosity will provide more gas diffusion path, which is favored for the oxygen reduction process. This novel nano-network microstructure with enlarged surface area, continuous conducting path, and high porosity is expected to significantly enhance the cathode performance because oxygen reduction is believed to occur at the TPBs where oxygen ions, electrons, and oxygen molecules are available.

3.2. Nano-network formation

In order to reveal the possible process for the nano-network formation, nitrates for SSC were mixed and heated in a mechanical convection oven with transparent windows. The nitrates melted at about 100 °C and decomposition started at about 230 °C. The decomposition yielded solid phase (oxides) in the mother liquid phase. The formation of solid particles can be described as a process of nucleation and growth. When the nitrates in bulk were decomposed in an alumina crucible, the products were of submicron in size regardless of the heating rates since growth could be conducted sufficiently (Fig. 2a). However, the decomposition process of the impregnated nitrates should be different since prior to decomposition, a thin layer of liquid film would be formed on the inner surface of the SDC frame. Grain growth within the liquid thin-film should be kinetically suppressed since the substance available for the growth is limited by the amount of the impregnated nitrates per surface area. Oxide nanobeads are consequently formed when the impregnated nitrates were decomposed (Fig. 2b). But the products are expected to be different in microstructure when the decomposition, which needs heat to complete the reaction, is performed with the different heating rates. At a low heating rate, the decomposition is expected to proceed slowly and uniformly. Thus there is more time for the solid nucleation and growth, resulting in relatively big particles that are distributed randomly on the inner surface of the SDC frame. At a high heating rate, temperature much higher than the thermodynamically decomposition temperature could be

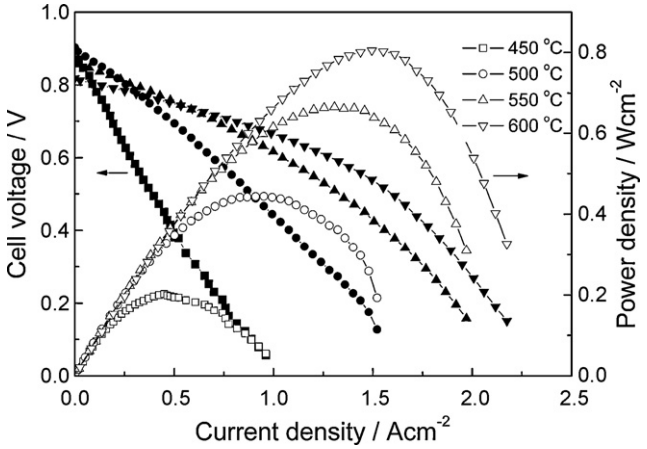

Fig. 3. Cell voltage (solid symbols) and power density (open symbols) as a function of current density for a single cell with a cathode as shown in Fig. 1b when humidified H_2 (3% H_2O, 60 ml min^{-1}) was used as the fuel and ambient air as the oxidant.

Table 1
Peak power density (P), ohmic resistance (R_o), and interfacial polarization resistance (R_p) at 500 °C for SOFCs with hydrogen as the fuel

P (W cm^{-2})	R_o (Ω cm^2)	R_p (Ω cm^2)	Cell components			Reference
			Cathode	Electrolyte	Anode	
0.15	0.50	0.68	SSC-GDC	20 μm GDC	Ni-GDC	[13]
0.19	0.48	1.0	SSC-SDC	30 μm SDC	Ni-SDC	[14]
0.25	0.40	0.50	SSC-SDC	18–20 μm SDC	Ni-SDC	[15]
0.21	0.67	0.79	SSC-SDC	25 μm SDC	Ni-SDC	[16]
0.44	0.20	0.21	SSC nano-network	10 μm SDC	Ni-SDC	This work

reached before the decomposition is started. The high temperature gradient might promote fast nucleation reactions, resulting in increased amount of nucleus, and thus the particle size decreases. Meanwhile, nucleation could be induced by the preformed nucleus. Growth of the neighboring nucleus leads to the formation of the nano-network with interconnected nanowires (Fig. 2c).

3.3. Single cell performance

The performance of the cathode prepared at a heating rate of 10 °C min^{-1} was investigated on a single cell with a Ni–SDC anode and a 10-μm thick SDC electrolyte. Humidified H_2 (3% H_2O) was supplied as the fuel and ambient air as the oxidant. The open-circuit voltage (V_{oc}) is lower than 1.0 V, and increases with the decrease of the operation temperature since doped ceria is not a pure oxygen ion conductor [12]. Peak power densities of 0.44 and 0.81 W cm^{-2} were achieved at 500 and 600 °C, respectively (Fig. 3).

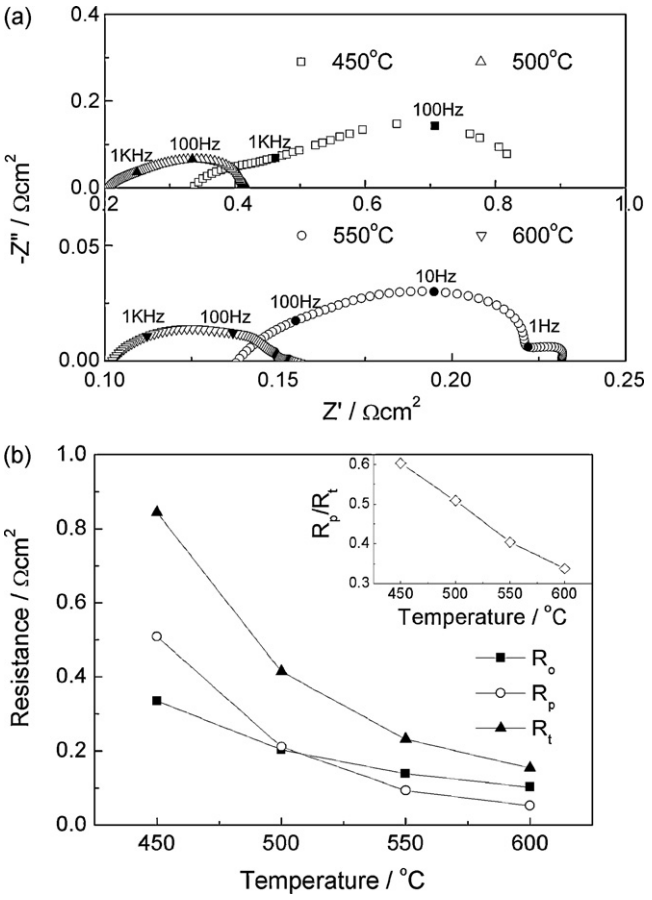

Fig. 4. (a) Impedance spectra of the cell measured under open-circuit conditions and (b) the total cell resistance (R_t), interfacial polarization resistance (R_p), and ohmic resistance (R_o) as determined from the impedance spectra. R_p/R_t is also shown in Fig. 4b.

These values are much higher than those for similar cells with SSC and doped ceria as the cathodes (Table 1) [13–16]. They are also much higher than those with $La_{0.8}Sr_{0.2}Co_{0.2}Fe_{0.8}O_{3-\delta}$ (LSCF) composites, which were reported to be a promising candidate as the cathodes for intermediate-temperature SOFCs [17,18]. With LSCF composite cathode, peak power density of 0.16 W cm^{-2} was achieved at 500 °C when 10-μm thick gadolinia doped ceria was used as the electrolyte [18]. In addition, the fuel cell performance is comparable to those achieved with the highest catalytic active material, $Ba_{0.5}Sr_{0.5}Co_{0.8}Fe_{0.2}O_{3-\delta}$ (BSCF), whose electrochemical surface exchange activity is 10 times as high as that of SSC [19,20]. However, the stability of BSCF cathode under fuel cell operating conditions is questionable since BSCF is susceptible to CO_2 even with relatively small quantities at the temperature range of 450–750 °C [21].

AC impedance spectra of the cell under open-circuit conditions are plotted in Fig. 4a. The total cell resistance (R_t), ohmic resistance (R_o), and interfacial polarization resistance (R_p) as determined from the impedance spectra at different temperatures are shown in Fig. 4b. The ratio of R_p to R_t increases with a decrease in the operating temperature, from 34% at 600 °C to 60% at 450 °C, implying that the cell performance is limited by both the ohmic resistance and the interfacial polarization resistance, which is originated from the cathode and the anode. Further analysis shows that R_t is primarily dominated by R_p below 500 °C and by R_o above 500 °C. At 500 °C, R_p has a similar value to R_o, and is close to 0.21 Ω cm^2, which is the lowest ever reported for single cells with SSC-based cathodes, as shown in Table 1. Since the anodes for all the different single cells are almost the same, the significantly lower R_p observed in this work might be attributed to the improved cathode performance due to the unique nano-network microstructure providing large surface area, high porosity, and enhanced ionic and electronic conducting property. It is noted that R_p at 500 °C for the SSC cathode is even lower than that of a cell with a BSCF–SDC composite cathode at the same operating temperature [22].

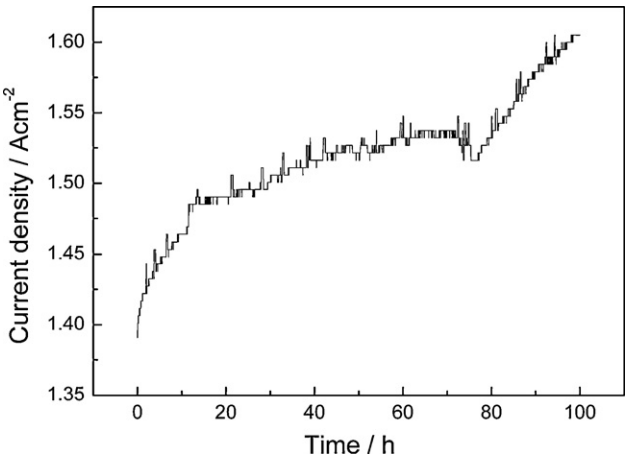

Fig. 5. Current density versus operating time with a constant voltage output of 0.5 V.

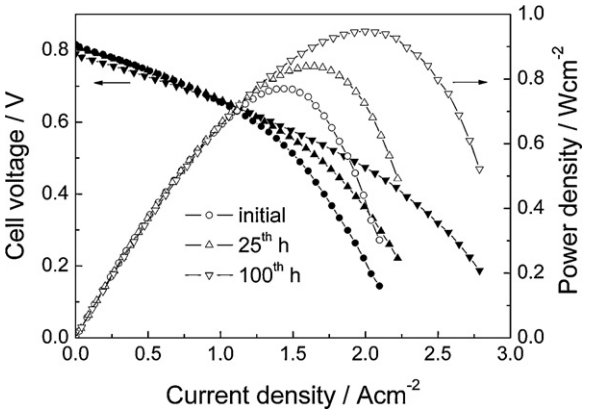

Fig. 6. Cell performance measured at 600 °C at different testing time.

To further investigate the cathode performance, a constant voltage of 0.5 V was maintained on the cell at 600 °C for 100 h. *V–I* curves and AC impedance spectra were measured at the initial, the 25th hour and the end of the durability test. It was found that under the potentiostatic treatment, the current density increased from 1.40 to 1.60 A cm^{-2} in 100 h (Fig. 5). The increase in current density indicates that no degradation occurred for the cathode. On the contrary, it shows enhanced cathodic performance upon cell operation. The improved activity can be further demonstrated from the *V–I* curves measured at the different cell operating time (Fig. 6). The peak power density increased from an initial value of 0.77 to 0.84 W cm^{-2} after 25-h operation, and to 0.95 W cm^{-2} after 100-h operation. The enhancement of the cell performance under operation can be further revealed from the impedance spectra measured under open-circuit conditions at different cell operation intervals as shown in Fig. 7. It is found that R_p decreases with time under the constant voltage load while R_o was almost invariant, indicating that the increase in power density is due to the improved activity of the electrode processes. R_t had an initial value of 0.159 Ω cm^2 and decreased to 0.148 Ω cm^2 after 100-h operation. These values are consistent with the corresponding cell resistances, which was 0.148 Ω cm^2 initially and 0.134 Ω cm^2 after 100-h operation estimated from the *V–I* curves in the low current range. Post-test microstructure investigation shows that the improvement in cell performance under cell operation might be caused by the cathode since its microstructure evolved over time while the anode microstructure was essentially unchanged. As shown in Fig. 1b, the fresh cathode possesses nano-network structure consisted of discrete nanowires made from SSC nanobeads and the boundaries between the nanobeads can be clearly identified. Under the cell operation, although the SSC cathode nano-network structure has maintained, the boundaries

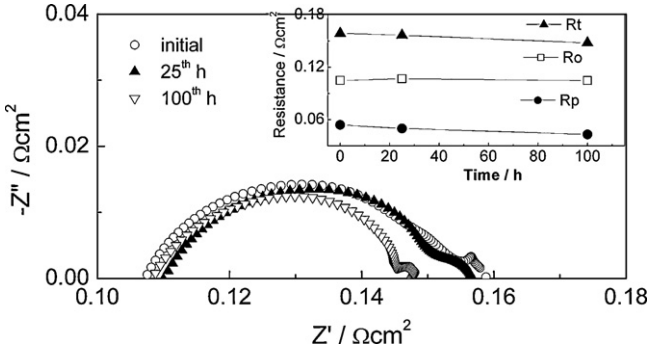

Fig. 7. Impedance spectra measured at 600 °C at different testing time.

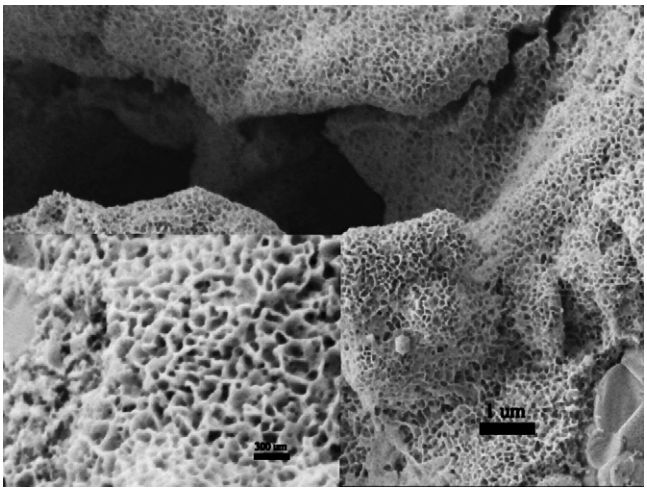

Fig. 8. Cross-sectional microstructure view for the cathode after the durability test.

between the SSC nanobeads disappeared and the SSC nanobeads merged (melted) into cross-connected nanowires whose diameter was close to that of the fresh nanobeads (Fig. 8). The disappearance in boundaries might be caused by heating at 600 °C as well as the cathodic polarization/current treatment, which has already been shown to cause substance diffusion [10,23]. The cathode microstructure evolvement might have resulted in a strengthened nano-network, showing better mixed-ionic–electronic conducting capability than that of the initial nano-network. Consequently, reduced R_p was obtained upon cell operation. In addition, Fig. 8 shows the evolved nano-network is more porous than the initially fresh one. Meanwhile, there was no observable difference in the anode microstructure at different testing duration while the porosity on the nano-network cathode increased during the fuel cell operation. Therefore, the effect of the anode on the polarization concentration should be invariable during the cell operation with a steady feed flow rate of H_2. In addition, the hydrogen utilization was relatively low during the *V–I* curve measurement (not more than 10% at the peak current) and the influence of concentration polarization on the anode is expected to be insignificant. Consequently, lower concentration polarization loss as indicated with the *V–I* curves (Fig. 6) measured at high current density seems to be due to the improved cathode gas diffusion as a consequence of the cathode microstructure evolution during the cell operation.

4. Conclusions

Nano-network structured $Sm_{0.5}Sr_{0.5}CoO_{3-\delta}$ cathodes for intermediate-temperature SOFCs have been successfully fabricated by simply increasing the rate to heat the precursor nitrates deposited from a well-developed ion-impregnation process. The cathodes are consisted of oxide nanowires formed from the nanobeads of less than 50 nm in diameter thus exhibiting large surface area and high porosity, forming straight path for ion and electron conduction, and consequently showing remarkably low interfacial polarization resistances. Change in the firing rate has found to be a highly effective approach to the fabrication of high-performance nano-network electrodes for intermediate-temperature SOFCs, producing the lowest interfacial polarization resistances (0.21 Ω cm^2 at 500 °C and 0.052 Ω cm^2 at 600 °C) ever reported for the SSC cathode materials. An anode-supported cell with 10-μm thick SDC electrolyte demonstrated a peak power density of 0.44 W cm^{-2} at 500 °C, which is also the highest ever reported for the SSC electrodes. Durability test showed that the

cathode performance increased with the operating time probably due to the cathode microstructure evolution to higher porosity to optimize the gas diffusion and well-connected SSC nanowires to strengthen ionic and electronic conducting path. Although the long-term stability and formation mechanism of the nano-network electrodes are yet to be further determined, the results indicate a new direction to significantly improve the performance of intermediate temperature SOFCs.

Acknowledgements

This work was supported by the Natural Science Foundation of China (50672096 and 50730002) and the Ministry of Science and Technology of China (2007AA05Z151).

References

[1] B.C.H. Steele, A. Heinzel, Nature 414 (2001) 345–352.
[2] Z.P. Shao, S.M. Haile, Nature 431 (2004) 170–173.
[3] Y.L. Zhang, S.W. Zha, M.L. Liu, Adv. Mater. 17 (2005) 487–491.
[4] T.Z. Sholklapper, H. Kurokawa, C.P. Jacobson, S.J. Visco, L.C. De Jonghe, Nano Lett. 7 (2007) 2136–2141.
[5] S.P. Jiang, Mater. Sci. Eng. A 418 (2006) 199–210.
[6] Y.Y. Huang, K. Ahn, J.M. Vohs, R.J. Gorte, J. Electrochem. Soc. 151 (10) (2004) A1592–A1597.
[7] F. Zhao, R.R. Peng, C.R. Xia, Mater. Res. Bull. 43 (2008) 370–376.
[8] K. Yamahara, C.P. Jacobson, S.J. Visco, L.C. De Jonghe, Solid State Ionics 176 (2005) 451–456.
[9] S.P. Jiang, Y.J. Leng, S.H. Chan, K.A. Khor, Electrochem. Solid-State Lett. 6 (4) (2003) A67–A70.
[10] T.Z. Sholklapper, V. Radmilovic, C.P. Jacobson, S.J. Visco, L.C. De Jonghe, Electrochem. Solid-State Lett. 10 (4) (2007) B74–B76.
[11] R.R. Peng, C.R. Xia, Q.X. Fu, G.Y. Meng, D.K. Peng, Mater. Lett. 56 (2002) 1043–1047.
[12] K. Eguchi, T. Setoguchi, T. Inoue, H. Arai, Solid State Ionics 52 (1992) 165–172.
[13] C.R. Xia, M.L. Liu, Solid State Ionics 144 (2001) 249–255.
[14] C.R. Xia, F.L. Chen, M.L. Liu, Electrochem. Solid-State Lett. 4 (5) (2001) A52–A54.
[15] X. Zhang, M. Robertson, S. Yick, C. De Petit, E. Styles, W. Qu, Y.S. Xie, R. Hui, J. Roller, O. Kesler, R. Maric, D. Ghosh, J. Power Sources 160 (2006) 1211–1216.
[16] Z.C. Wang, W.J. Weng, K. Chen, G. Shen, P.Y. Du, G.R. Han, J. Power Sources 175 (2008) 430–435.
[17] N. Oishi, A. Atkinson, N.P. Brandon, J.A. Kilner, B.C.H. Steele, J. Am. Ceram. Soc. 88 (6) (2005) 1394–1396.
[18] Y.J. Leng, S.H. Chan, S.P. Jiang, K.A. Khor, Solid State Ionics 170 (2004) 9–15.
[19] Y.H. Zhang, X.Q. Huang, Z. Lu, Z.G. Liu, X.D. Ge, J.H. Xu, X.S. Xin, X.Q. Sha, W.H. Su, J. Power Sources 160 (2006) 1217–1220.
[20] F.S. Baumann, J. Fleig, G. Cristiani, B. Stuhlhofer, H.-U. Habermeier, J. Maier, J. Electrochem. Soc. 154 (9) (2007) B931–B941.
[21] A.Y. Yan, M.J. Cheng, Y.L. Dong, W.S. Yang, V. Maragou, S.Q. Song, P. Tsiakaras, Appl. Catal. B: Environ. 66 (2006) 64–71.
[22] N. Ai, Z. Lu, K.F. Chen, X.Q. Huang, B. Wei, Y.H. Zhang, S.Y. Li, X.S. Xin, A.Q. Sha, W.H. Su, J. Power Sources 159 (2006) 637–640.
[23] S.P. Jiang, J.Solid State Electrochem. 11 (2007) 93–102.